Book of Tutorials and Abstracts

European Microbeam Analysis Society

EMAS 2026

15th

REGIONAL WORKSHOP

TOPICAL CONFERENCE ON ELECTRON BACKSCATTER DIFFRACTION (EBSD)

14 to 17 June 2026
at the
CentraleSupélec, Gif-sur-Yvette, France

Organised in collaboration with:
ICMMO, ENS Paris-Saclay,
Université Paris-Saclay

EMAS
European Microbeam Analysis Society eV
www.microbeamanalysis.eu/

This volume is published by:
European Microbeam Analysis Society eV (EMAS)
EMAS Secretariat
c/o Eidgenössische Technische Hochschule, Department of Earth and Planetary Sciences
Clausiusstrasse 25
8092 Zürich
Switzerland

ISBN 978 90 8227 6992
NUR code: 971 – Materials Science

TRANSMISSION KIKUCHI DIFFRACTION IN PRACTICE: PRINCIPLES, CHALLENGES AND EMERGING OPPORTUNITIES

Alice Bastos da Silva Fanta

Technical University of Denmark, Microstructural Analysis of Materials Processes
Fysikvej, Bldg. 307, 2800 Kgs. Lyngby, Denmark
e-mail: absf@dtu.dk

Alice Bastos da Silva Fanta have studied materials science with specialisation on metallic materials at the Technische Universität Berlin, Germany finishing her studies in 2003. It was first on her PhD from 2004 to 2007 at the Max-Planck-Institute für Eisenforschung GmbH (MPIE) in Düsseldorf that she was introduced to EBSD by Dr Stefan Zaefferer. In 2008 she moved to Denmark and became responsible for application and developments of EBSD at the microscopy centre at the Technical University of Denmark. She has not left the technique since and is currently a senior researcher at DTU Nanolab focussing on characterising nanocrystalline and low dimensional materials with transmission Kikuchi diffraction (TKD) in the SEM and on further developing the technique. Currently she is also working on exploring the use of MEMS-heating devices to investigate microstructure dynamics in the SEM with both EBSD and TKD and the applications of liquid cell devices to study particle dynamics in liquid.

1. BACKGROUND

The power of investigating electron transparent specimens in the SEM using a conventional electron backscatter detector (EBSD) was first demonstrated in the pioneering work of Keller and Geiss in the early 2010s [1, 2]. They introduced the method under the name transmission electron backscatter diffraction (t-EBSD) and although this original terminology still appears in the literature, the technique is now most widely known as transmission Kikuchi diffraction (TKD), because the Kikuchi diffraction patterns arise from the forward-scattered transmitted electrons, distinguishing it from the surface-based backscattered patterns of EBSD. TKD relies on the automated acquisition of these forward-scattered Kikuchi diffraction patterns from electron transparent samples with a standard EBSD detector. By replacing the large interaction volume associated with the conventional tilted-bulk EBSD geometry with the much smaller interaction volume of a flat (or only slightly tilted) electron transparent sample, TKD achieves one order of magnitude improvement in spatial resolution [3, 4] for crystallographic orientation mapping in the SEM.

Over time, TKD became widely recognised for its capabilities of characterising a broad range of nanocrystalline materials in the SEM. As the technique matured, instrumental developments such as the introduction of exchangeable detector heads allowing to change the position of the detector screen from the traditional side-mounted (off-axis configuration) to a position directly beneath the electron-transparent sample (on-axis and near-axis configuration) [5, 6] (Fig. 1) fundamentally improved the TKD setup. This geometric change enables higher signal yield; less geometric distortions associated with the steep gnomonic projection inherent to off-axis TKD and ultimately further improves the spatial resolution [5, 7, 8].

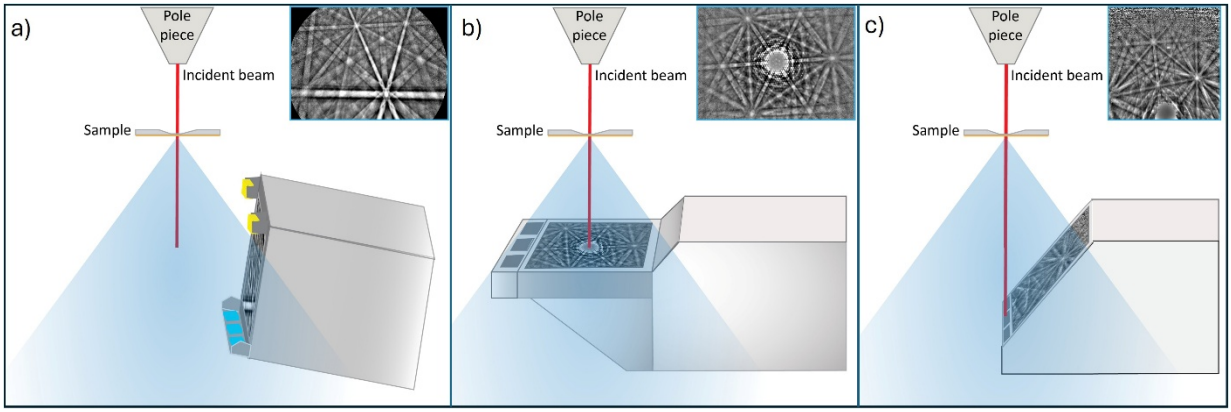

Figure 1. Schematic representation of the TKD detector configuration and corresponding diffraction patterns; a) off-axis; b) on-axis; c) near-axis.

TKD has been widely used to characterise nanocrystalline structures in a large variety of fields, such as metallurgy [9-11], functional materials [12-16], geology [17-19] and biomaterials [20].

Most of these applications focussed on exploring the additional spatial resolution achieved with the method in comparison to EBSD. TKD plays also an important role in the fabrication of atom probe tomography (APT) samples, as it can provide real-time microstructure feedback during specimen preparation in the focussed ion beam (FIB) instrument, allowing accurate targeting of microstructure features for APT analysis [21-24].

Transmission Kikuchi diffraction, like EBSD, relies on the formation and analysis of Kikuchi diffraction pattern. The key distinction between the two techniques lies in the required sample thickness and the location where the diffraction signal originates. In TKD a finely focussed electron beam enters the electron-transparent thin specimen and undergoes both inelastic and elastic scattering events. The inelastic interaction creates an incoherent point source within the sample, from which the electrons are subsequently Bragg-diffracted by the crystal planes and Kikuchi lines are observed as the projection of the crystal lattice planes on the detector screen positioned beneath the sample. Since the TKD samples are thin, the interaction volume is reduced, being constrained by the foil thickness and by the position of the deepest thermal diffuse scattering (TDS) event, which sharply limits signal convolution from overlapping grains and phases. As a result, TKD resolution is governed by parameters that control electron scattering and escape, including foil thickness, material scattering properties (e.g., Z-dependent TDS and elastic mean free paths), and accelerating voltage, all of which determine where in the foil patterns originate and how sharply Kikuchi bands form.

2. TKD IN PRACTICE

2.1. Detector

Two major detector geometries are commonly used in TKD [25, 26]. In the conventional off-axis configuration, the EBSD phosphor screen is placed in the standard reflection geometry position, laterally offset and tilted relative to the electron beam (Fig. 1a). This arrangement captures only a fraction of the forward-scattered electron cone resulting in stronger gnomonic distortions and varying pattern intensity (see pattern insert in Fig. 1a), typically requiring higher beam currents and longer exposure times to obtain reliable indexing. Some geometry adjustments, such as reducing the working distance, slightly tilting the sample or optimising the detector distance and tilt angle can improve effective collection of forward-scattered electrons, as they increase the solid angle delimited by the detector (see Fig. 4). The on-axis configuration [5] repositions the scintillator directly below the thin sample and perpendicular to the incident beam, analogous to the geometry used in TEM (Fig. 1b). This geometry enables collection of the complete high-intensity forward-scattered electron distribution, which significantly enhances the diffraction signal and reduces geometric distortion. It has been demonstrated [7, 8] that on-axis geometry enables up to twenty-fold reduction in electron dose or acquisition time while maintaining equivalent pattern quality and indexing reliability, making it particularly advantageous for beam sensitive materials and large area mapping. However, the on-axis

geometry requires a dedicated on-axis detector head, implying both additional equipment investment and time spent exchanging between the two detector head configurations (in case of switching between EBSD and on-axis TKD). Moreover, the direct and intense un-scattered primary electron beam also reaches the detector screen, leading to high intense signal in the centre of the patterns (see pattern inserted in Fig. 1b). The intense direct beam signal can saturate the phosphor screen and limit the maximum usable beam current, as its central intensity greatly exceeds that of the peripheral Kikuchi patterns. Recently, a new variant of detector head was introduced called near-axis TKD [6, 14] (Fig. 1c), in which a tilted screen is positioned close to the beam axis in a way that it still intercepts the intense forward-scattered electron while preventing the primary beam from striking the phosphor screen directly, thus preserving most of the advantages of on-axis TKD.

2.2. Sample

Preparing samples for TKD is considerably more challenging than for EBSD, because it requires electron transparent foils with minimal surface damage and controlled thickness. Focussed ion beam (FIB) lift-out is the most widely used approach, as it provides site-specific sample preparation, accurate geometry control and the possibility to directly correlate EBSD and TKD results captured from the same reason of interest. However, surface amorphisation [27], implantation damage, curtaining as well as redeposition, can degrade Kikuchi pattern quality.

Another commonly used approach is jet-electropolishing the samples, where the foil is thinned anodically until it finally forms a hole surrounded by a thin annular region suitable for TKD analysis. While this technique can produce larger electron transparent samples, in comparison to FIB lamella, it also introduces thickness gradients which can reduce spatial resolution and make reliable indexing more challenging. A further drawback is the limited control over the exact region sampled. Other TEM sample preparation methods, such as carbon replicas [28], drop-casting nanoparticles dispersed in liquid onto lacey-carbon TEM grids [29], ultramicrotomy [14] and direct deposition of thin film onto electron transparent membranes [30, 31] are recognised routes to prepare TKD specimens.

In TKD, sample thickness is a key parameter controlling pattern quality and indexability [32-34]. Both insufficient and excessive thickness degrade the Kikuchi pattern quality in distinct ways. Figure 2 shows on-axis TKD patterns acquired from an yttria stabilised zirconia (YSZr) fibre with thickness decreasing from ~ 300 nm at position 1 to ~ 15 nm at position 6, illustrating the progressive disappearance of Kikuchi lines and bands with decreasing thickness and the loss of spot diffraction patterns with increasing thickness. If the sample is too thin, the number of thermal diffused scattering (TDS) events becomes too low to sustain the dynamical scattering required for Kikuchi-band formation, thus only spot patterns are observed in the detector screen [33] (Fig. 2 - position 6). At the opposite extreme, too thick specimens introduce more inelastic and diffuse scattering, increasing background intensity, causing contrast degradation or even contrast inversion [35]. Moreover, beam broadening increases with sample thickness and results

in reduced spatial resolution (see Fig. 3). The optimal thickness is dictated by the material's scattering cross-section (linked to atomic number and density) and by the accelerating voltage, which sets the electron mean free path and the effective depth of dynamical scattering. Liu *et al.* [36] proposed that the information depth is governed by the TDS mean free path (λ_{TDS}) suggesting that sample thickness should not exceed $6\lambda_{TDS}$ for high symmetry crystals and $\leq 3\lambda_{TDS}$ for lower-symmetry ones. Brodu *et al.* [33] investigated the influence of sample thickness and electron beam energy on the appearance and disappearance of spot diffraction pattern and on the contrast of the Kikuchi patterns, proposing a model based on the plasmon and phonon mean free path to guide experiments toward reliable Kikuchi pattern indexing. Recently a solution to improve indexing of contrast inverted Kikuchi patterns was proposed [37] suggesting that sample upper thickness limit might be extended by improving indexing routines.

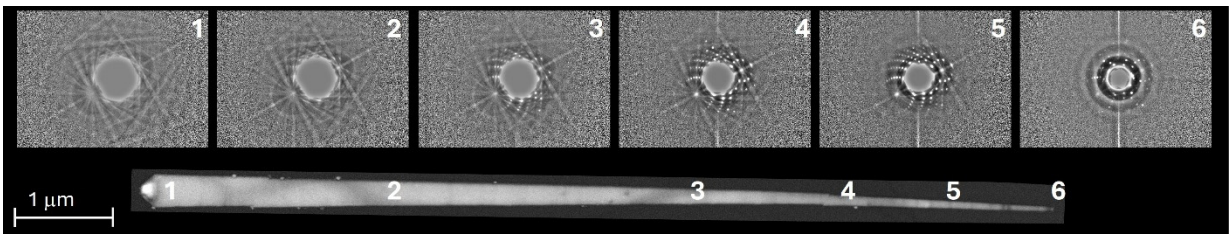

Figure 2. On-axis TKD patterns from an YSZr fibre as a function of local thickness ranging from approx. 300 nm (position 1) to 15 nm (position 6). All patterns acquired with the same microscope parameters.

2.3. Microscope parameters

2.3.1. Beam energy. The accelerating voltage influences both the quality of the TKD patterns and the spatial resolution, because it directly controls the electron mean free path, the balance between elastic and inelastic scattering and the beam spread along the interaction volume of the thin specimen. As monte Carlo simulations using CASINO [38] shows in Fig. 3 the higher the beam energies the tighter the beam profile through the foil is, improving pattern contrast and spatial resolution, whereas lower energies increase scattering angles and cause more rapid broadening. Consequently, most TKD experiments are performed at primary beam energies of 30 kV, unless due to too thin specimen or very low atomic number composition only spot diffraction patterns are formed at this high energies [33, 39, 40].

2.3.2. Beam current. The beam current influences both the effective probe size during microstructural scanning and the signal collection efficiency at the detector. Conventionally, a balance must be found between spatial resolution, signal intensity, and acquisition speed. The optimal beam current depends also strongly on the detector geometry. In the off-axis TKD configuration, high beam currents are required to increase signal yield at the detector. In contrast,

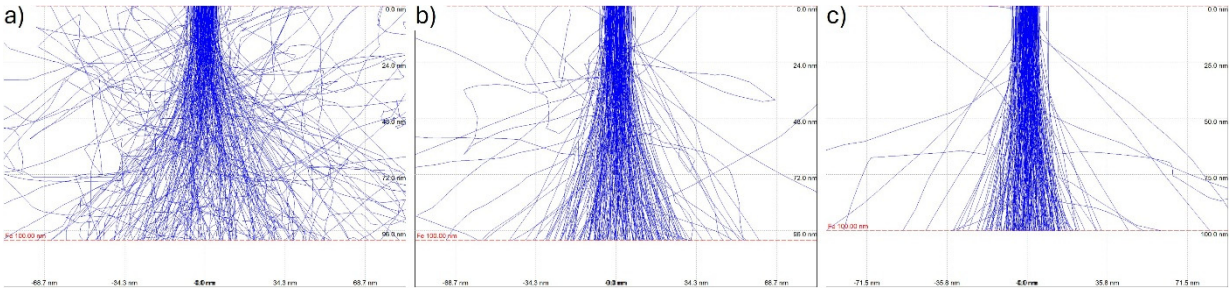

Figure 3. Monte Carlo simulation of electron trajectories in an Fe-based sample with 100 nm thickness at three different accelerating voltages: a) 10 kV, b) 20 kV, and c) 30 kV, considering 5,000 electrons and a 10 nm beam radius [38].

in on-axis TKD, excessively high beam currents can saturate the detector due to the intense direct beam, obscuring large areas of the phosphor screen and thereby hindering reliable Kikuchi pattern indexing.

2.3.3. Working distance. Reducing the working distance can be favourable for increasing the signal collection in the off-axis TKD configuration (see Fig. 4), while in on-axis and near-axis TKD the working distance plays a minor role in the signal intensity, but can be used to adjust the detector distance between sample and detector, thus increasing or decreasing the collection angle.

2.3.4. Detector distance/tilt. The detector distance, as in EBSD, determines the angular collection range of the diffracted signal. Reducing the detector distance effectively zoom out the diffraction patterns, capturing a larger angular range so that more diffraction bands and zone axis are visible for indexing, while reducing the number of pixels per band width. Increasing the detector distance has the opposite effect, providing higher angular resolution at the expense of angular coverage. Depending on the detector design, the effective detector distance can be adjusted by tilting the detector assembly toward (up) or away (down) from the sample (see Fig. 4b). The optimal detector position strongly depends on the analytical objective, such as maximizing phase discrimination or achieving high angular resolution.

2.3.5. Sample tilt. Sample tilt is only required when performing TKD orientation mapping with an off-axis detector. The tilt of the sample, in opposite direction to the detector, is predominantly used to enhance signal yield (see Fig. 4a). However, it also influences the interaction volume, changing its shape from circular to elliptical, and the effective path of the electron within the sample [3, 40]. Figure 4 shows an illustration of the effect of changing the sample tilt and the working distance in the a) off-axis TKD configuration, and b) the effect of changing detector tilt and thereby detector distance in on-axis TKD.

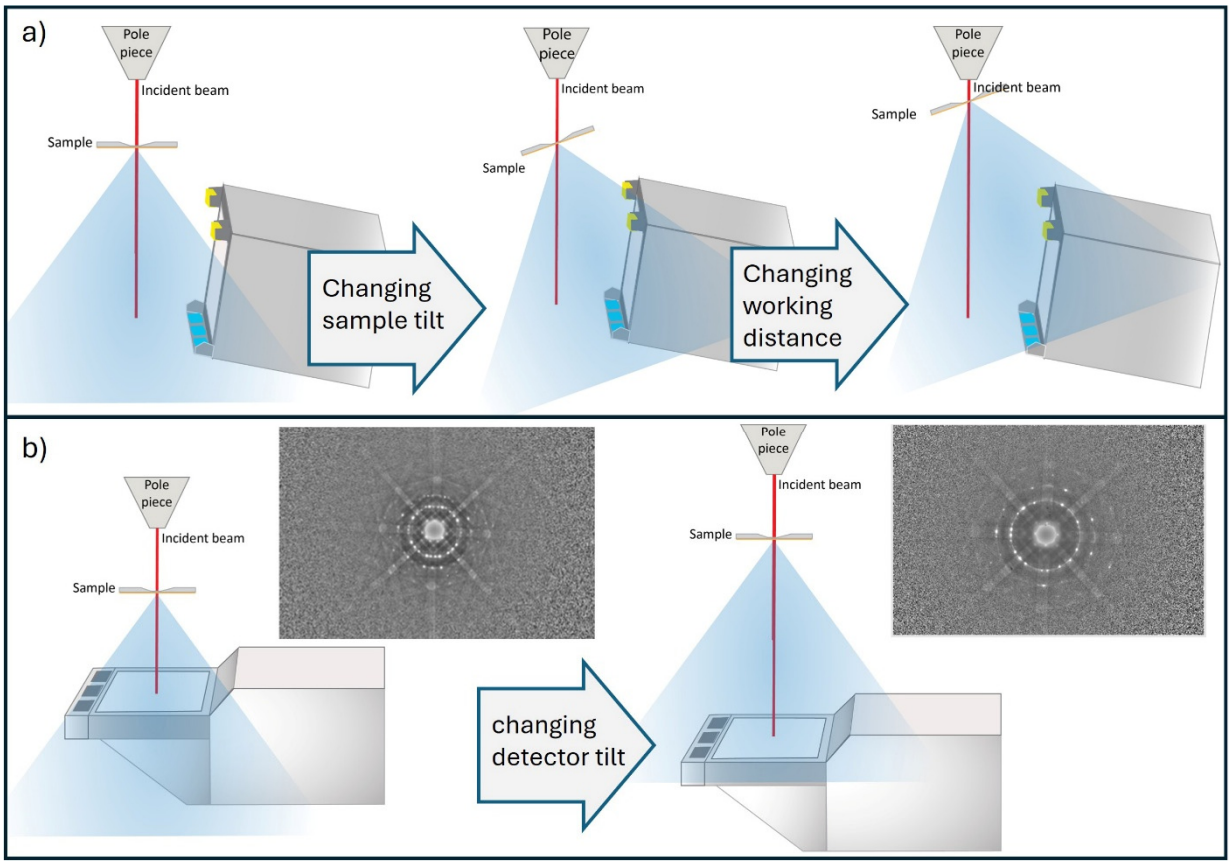

Figure 4. Schematic illustration of changes in sample tilt (from 0° to -20°) and working distance in a) off-axis TKD, and b) of changes in detector tilt for on-axis TKD.

2.4. Spatial resolution (lateral and depth)

Spatial resolution is the biggest advantage of TKD in comparison with EBSD. In TKD the spatial resolution is governed by a combination of lateral broadening inside the foil and the exit-surface limited information depth. It is controlled by a combination of intrinsic materials properties and extrinsic microscope parameters. Reports on spatial resolution range from 2 nm [4] to 10 nm [2, 7], depending on material, conditions and approach.

When discussing spatial resolution in EBSD and TKD, we commonly differentiate between physical (PSR) and effective spatial resolution (ESR). The physical refers to the smallest interaction volume that can generate a unique Kikuchi pattern, whereas the effective spatial resolution is defined by the ability of the indexing routine to differentiate between distinct diffraction signals within a diffraction image [7, 41]. PSR in TKD is limited by beam broadening inside the foil therefore it depends primarily on foil thickness, accelerating voltage, and atomic number (Z) and to some extent on the probe size. Effective lateral resolution is commonly better than physical; however, it depends strongly on the quality of the patterns acquired. Consequently, detector geometry and pattern signal to noise ratio also plays an important role. The ESR plays a significant role for the indexing accuracy across grain boundaries, however,

it has less significance for differentiating crystal rotation within deformed structures [42]. Comparative experiments between on-axis and off-axis TKD reveals slightly improved spatial resolution in the on-axis configuration ~ 6 nm in contrast to ~ 9 - 10 nm under identical conditions [43]. Whereas the ESR improvement stems from capturing a larger fraction of the forward-scattered cone with lower geometric distortion, yielding higher band contrast at lower dose.

Particularly for TKD, it is also necessary to subdivide the PSR in lateral-PSR and depth-PSR, as the depth from where the signal originates plays a role on the resulting microstructure. As previously demonstrated by Rice *et al.* [32] the detectable TKD intensity originates very near the beam exit surface. Figure 5 shows such example, where TKD maps were conducted on a 20 nm Au film deposited on a TEM window with a 5 nm Si_3N_4 membrane, with GaAs-nanowires dispersed on top of the Si_3N_4 membrane (see sketch in Fig. 5). By mapping the area where the nanowires are facing the incoming beam, the Au microstructure is fully resolved (Fig. 5a), but when the nanowires are on the exit surface (Fig. 5b), the GaAs-nanowire crystal orientation is revealed (please observe that Fig. 5b was flipped horizontally for better spatial correlation with Fig. 5a). This is further highlighted by the pattern embedded in the image. In particular, no overlapping patterns are observed in position 2a and 2b, and the pattern acquired at position 2a exhibits the same orientation as those obtained from position 1a and 1c. However, the signal to background ratio is lower at position 2a, consistent with the larger local sample thickness of approximately 125 nm compared to 25 nm in other regions. A similar behaviour is observed when the nanowire is located at the beam exit surface, however, in this case, the crystal structure at position 2b corresponds to the GaAs.

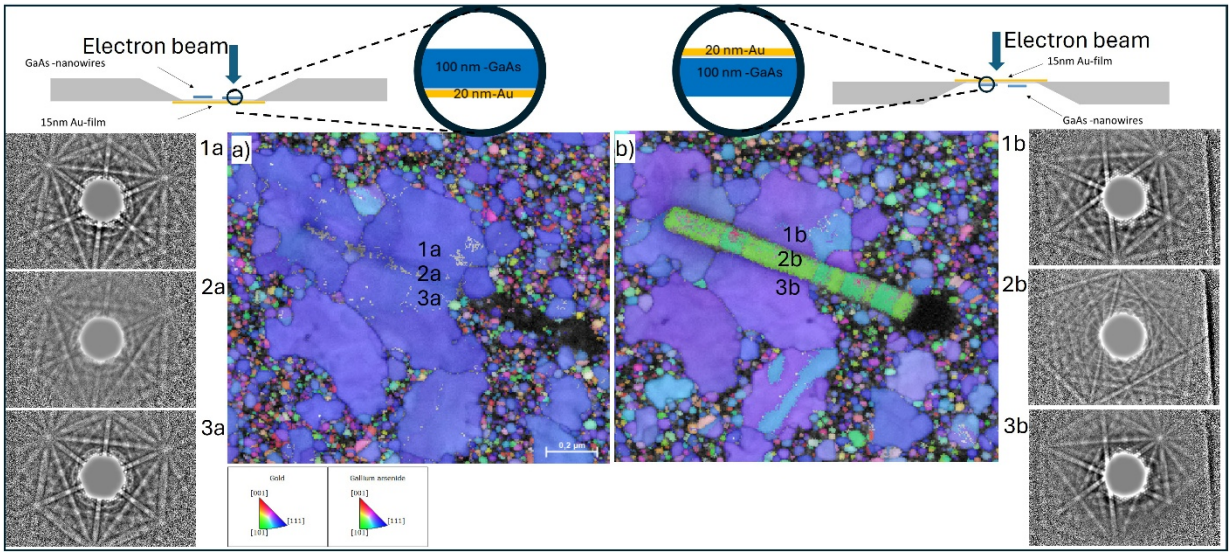

Figure 5. TKD orientation maps of an Au-GaAs layered structure created by dispersing GaAs nanowires onto a TEM window coated with a 20 nm Au film. a) and b) show the same area after flipping the sample: in a) the GaAs nanowire faces the incident electron beam, whereas in b) the Au film faces the beam. Orientation maps and corresponding diffraction patterns demonstrate that the GaAs nanowire is only detectable when located at the exit surface.

From the depth PSR perspective, carefully designed experiments demonstrate depth resolution of ~ 30 - 65 nm between 10 - 30 kV, which scales approximately linearly with beam energy and is material dependent [33, 36, 40]. Liu *et al.* [36] reported that the mean free path of thermal diffuse scattering is close related to the depth from which the Kikuchi signal arises and suggest a minimum and an ideal sample thickness for TKD analysis, depending on the sample composition. The depth of the signal is one of the larger differentials between the SEM and TEM based orientation mapping technique for nanocrystalline materials. While the spot patterns utilised in TEM orientation mapping give information about the entire sample cross-section, the Kikuchi diffraction signal basically only provides crystal information about the final layer of the sample cross-section.

To further improve the lateral spatial resolution of TKD it is necessary to either minimise the effective interaction volume and/or enhance the indexing robustness of overlapping patterns, for example by using newly developed approaches from Cios *et al.* [37]. One established route to improve image resolution in the SEM is to operate in immersion mode, in which the specimen is placed within the magnetic field used to form the probe [44]. This configuration reduces the probe size and the depth of focus; however, it also imposes constraints for magnetic materials and introduces distortions and shifts in the recorded Kikuchi patterns. Corrections schemes for this distortion have been proposed in the literature [45] and are implemented in several commercial EBSD/TKD software packages [46-48].

In presence of a strong magnetic field, the trajectories of scattered electrons are compressed toward the optical axis, which significantly reduces the ability of an off-axis detector to capture the transmitted signal, while on-axis detectors remain effective [48]. Figure 6a shows the PSR for a 20 nm thin Au sample at 30 kV acceleration voltage in both field-free and immersion mode at two different beam currents following the methodology presented by Niessen [7]. For both beam currents the PSR is significantly improved in immersion mode. Figures 6b and 6c presents the TKD maps of the same area of a 20 nm Au sample acquired in respectively field-free mode and in immersion mode. Closer inspection of the highlighted microstructural areas confirms that the reduced probe size in immersion mode enables more reliable indexing of the finer structural features.

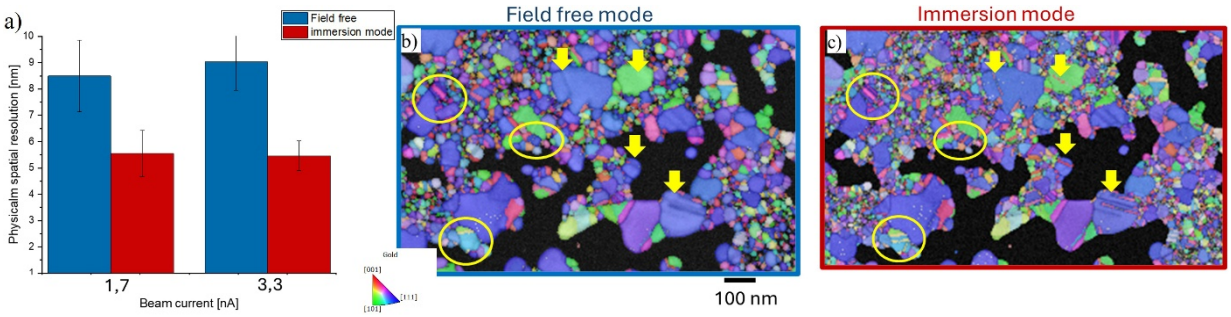

Figure 6. Improvement of the PSR for an Au sample in immersion mode in comparison to field-free mode; a) PSR as a function of the beam current and lens mode; b) and c) IPF-s map of the same location measured in b) field free, and c) immersion mode, with highlighted areas showing some features that are better resolved in immersion mode.

2.5. STEM images and TKD

Imaging diodes are commonly attached to the frame of most EBSD and TKD detectors and are used for direct imaging of forward- and backscatter electrons, providing high-contrast, real-space images that are sensitive to crystallographic orientations, topography and material contrast [49]. When using an off-axis geometry, the diodes located at the bottom of the EBSD detector frame can be used to generate dark-field (DF) images of the sample, with the effective collection angle tuneable through the insertion length of the detector [30, 50]. In on-axis and near-axis TKD geometry these diodes can be positioned directly beneath the thin specimen in the optical axis of the SEM, enable the independent collection of signals from each diode to generate bright-field (BF) and dark-field (DF) images of the specimen. Such scanning transmission images (STEM) are particularly effective for focussing the beam and navigation on the electron transparent samples. It is important to highlight that these STEM images results from the projection of the entire sample thickness [51], whereas TKD orientation maps primarily reflects the microstructure close to the exist surface. As a result, forward-scatter images and TKD mapping provide fundamentally complementary information. Moreover, the use of virtual apertures, implemented by integrating intensity over user-defined region of the detector plane, has been demonstrated, enabling a direct link between TKD with 4D-STEM approaches in the SEM [52-54].

3. CHALLENGES

In addition to the intrinsic and extrinsic parameters that govern the lateral and depth resolution of TKD, several practical challenges must be addressed to ensure reliable data acquisition. These include control of specimen charging, drift and carbon contamination.

Charging is commonly observed in thin electron transparent specimens supported by membranes that do not provide sufficient electrical conductivity to dissipate the incident beam charge (e.g., Si_3N_4 membranes). Mitigation strategies include operating the SEM in low-vacuum mode or applying a very thin conductive coating to the backside of the support film (see example in Figs. 7a and 7b). Drift effects are more pronounced when performing TKD in off-axis configuration, since long exposure times are required for increasing pattern intensity at the detector [7, 8]. Increasing beam current or step size may be required to avoid image distortion.

Carbon contamination represents one of the most common and challenging issues in TKD experiments. Hydrocarbons present within the SEM column or introduced during sample handling can crack under electron irradiation, progressively depositing carbon on the specimen. Effective mitigation strategies include plasma cleaning of the sample prior to TKD measurements and the use of low vacuum conditions to suppress hydrocarbon deposition during acquisition. However, for oxidation sensitive materials, conventional air or oxygen based plasma cleaning may alter the specimen surface and hydrogen based plasma cleaning provides an effective alternative [55].

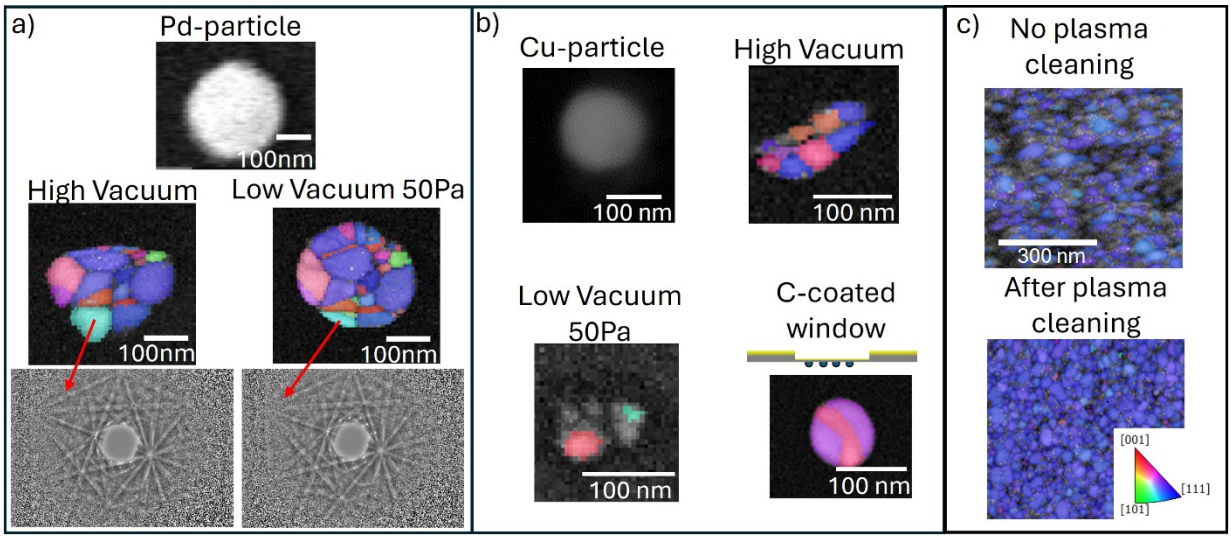

Figure 7. Examples of solutions to mitigate charging and improve indexing efficiency by a) increasing the chamber pressure, b) by adding a thin carbon coating to the Si_3N_4 TEM window, and c) by plasma cleaning of the sample prior to the TKD experiments.

Figure 7 illustrates several of these recommendations. In Fig. 7a shows the benefit of performing TKD mapping under low vacuum condition for a Pd nanoparticle supported on a Si_3N_4 membranes, where increasing the chamber pressure to 50 Pa effectively reduces charging without significantly degrading the quality of the Kikuchi patterns. In Fig. 7b similar approach was tested on a Cu nanoparticle, however it proved ineffective because of the oxidation of the particles during the experiments. To overcome this limitation, a thin carbon coating was applied on the membrane side of the sample to neutralize charging without altering the sample structure. Figure 7c shows the improved index efficiency achieved by plasma cleaning the sample prior to the TKD experiment.

4. EMERGING OPPORTUNITIES

Beyond its improvement in spatial resolution relative to EBSD, the true value of TKD lies in its advantages over TEM-based orientation mapping techniques. TKD retains the operational simplicity, automation capabilities, and high throughput characterisation inherent to SEM instrumentation, enabling multiple samples to be loaded, analysed, and processed through fully automated routines, thereby enabling high-throughput characterisation of nanocrystalline materials. In addition, because TKD is methodologically close related to EBSD, it can directly inherit the extensive ecosystem of EBSD software, pattern indexing algorithms, and established automation strategies, offering a level of robustness and accessibility that is not yet widely available for orientation mapping within the TEM. Moreover, TKD enables orientation mapping of FIB prepared lamellae without exposing them to air, thereby avoiding surface oxidation or contamination that might otherwise alter the sample. Because Kikuchi patterns in TKD originate

predominantly from the exit surface of the foil, they are less affected by overlapping grains signal, making fully automated orientation mapping in some cases more reliable than in TEM based precession or nanobeam diffraction workflows [29, 56].

TKD also opens opportunities that extend beyond the indexing of Kikuchi patterns. In principle, both Kikuchi and spot diffraction patterns could be simultaneously collected in the on-axis TKD detector. However, the limited dynamic range of the existing detectors complicates the capture of the combined signals (the direct transmitted beam is orders of magnitude more intense than the Kikuchi bands), consequently increasing exposure to enhance the weak features (Kikuchi bands) saturates the detector centre and covers the spot diffraction patterns (Fig. 8a). Approaches to overcome these limitations are under development and involve both hardware and software-based intensity management strategies [34, 57]. Figure 8 illustrates one such promising prospective solution, wherein adding a physical filter to the on-axis TKD detector screen enables simultaneous acquisition of spot and Kikuchi patterns is demonstrated. Once established, the capability of simultaneous capture and indexing of both types of signals will expand the range of sample thicknesses and material compositions that can be analysed directly in the SEM. Furthermore, this may open opportunities to explore beam-deflection-based contrast and access local electric or magnetic fields within the specimen, analogous to differential phase contrast (DPC) imaging [58]. Together, these opportunities position TKD not merely as a higher resolution version of EBSD, but as a flexible, accessible platform for transmission-based crystallography and mesoscale materials characterisation inside the SEM.

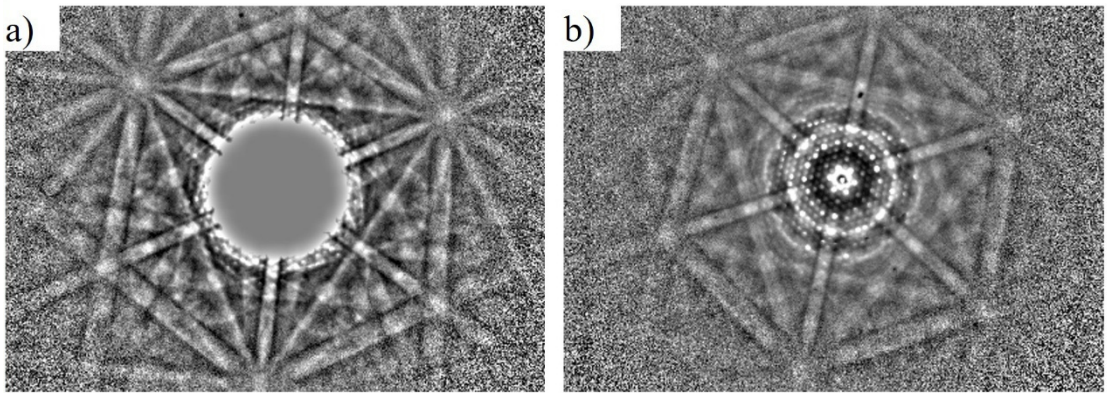

Figure 8. On-axis TKD pattern obtained from the same position in the sample and with the same microscope settings. a) Strong direct beam intensity saturates the detector and only Kikuchi patterns are acquired. b) A physical filter was introduced to control the dynamic range of the detector and allow acquisition of spot and Kikuchi patterns simultaneously.

5. REFERENCES

[1] Geiss R, Keller R and Read D 2010 *Microsc. Microanal.* **16** 1742-1743
[2] Geiss R H, Rice K P and Keller R R 2013 *Micros. Today* **21** 16-20

[3] Sneddon G C, Trimby P W and Cairney J M 2016 *Mater. Sci. Eng. R Reports* **110** 1-12
[4] Trimby P W 2012 *Ultramicroscopy* **120** 16-24
[5] Fundenberger J J, *et al.* 2016 *Ultramicroscopy* **161** 17-22
[6] Coleman M, *et al.* 2025 *Microsc. Microanal.* **31** 556-557
[7] Niessen F, Burrows A and Bastos da Silva Fanta A 2018 *Ultramicroscopy* **186** 158-170
[8] Yuan H, *et al.* 2017 *J. Microscopy* **267** 70-80
[9] Cayron C 2020 *Crystals* **10** 562
[10] Yoo Y S J, *et al.* 2021 *J. Mater. Res.* **36** 2754-2762
[11] Tokarski T, Cios G, Kula A and Bała P 2016 *Mater. Charact.* **121** 231-236
[12] Wickman B, *et al.* 2017 *Sci. Reports* **7** 40500
[13] Alekseeva S, *et al.* 2021 *Nat. Commun.* **12** 5427
[14] Barsoum M L, Abbott T M, Jacobsen S D, Farha O K and Dravid V P 2026 *Nano Lett.* **26** 2170-2176
[15] Lederer M, *et al.* 2020 *Nanomater.* **10** 384
[16] Barroo C, Akey A J and Bell D C 2019 *Appl. Surf. Sci.* **487** 1362-1365
[17] Jacob D E, Piazolo S, Schreiber A and Trimby P 2016 *Nat. Commun.* **7** 11891
[18] Daly L, *et al.* 2017 *Geochim. Cosmochim. Acta* **216** 42-60
[19] De Winter D A M, *et al.* 2013 *J. Struct. Biol.* **183** 11-18
[20] Koblischka-Veneva A, Koblischka M R, Schmauch J and Hannig M 2018 *Nano Res.* **11** 3911-3921
[21] Zschiesche H, *et al.* 2019 *Ultramicroscopy* **206** 112807
[22] Babinsky K, de Kloe R, Clemens H and Primig S 2014 *Ultramicroscopy* **144** 9-18
[23] Babinsky K, *et al.* 2015 *Ultramicroscopy* **159** 445-451
[24] Breen A J, et al. 20174 *Microsc. Microanal.* **23** 279-290
[25] Zhang T and Britton B 2025 *Microsc. Microanal.* **31** (Supplm. 1) ozaf048.283
[26] Zhang T, Berners L, Holzer J and Britton T 2025 *Mater. Charact.* **222** 114853
[27] Zieliński W, Płociński T and Kurzydłowski K J 2015 *Mater. Charact.* **104** 42-48
[28] Bocker C, Kracker M and Rüssel C 2014 *Microsc. Microanal.* **20** 1654-1661
[29] Mariano R G, Yau A, McKeown J T, Kumar M and Kanan M W 2020 *ACS Omega* **5** 2791-2799
[30] Bastos da Silva Fanta A, *et al.* 2019 *Ultramicroscopy* **206** 112812
[31] Heinig M F, Bastos da Silva Fanta A, Wagner J B and Kadkhodazadeh S 2020 *ACS Appl. Nano Mater.* **3** 4418-4427
[32] Rice K P, Keller R R and Stoykovich M P 2014 *J. Microscopy* **254** 129-136
[33] Brodu E, Bouzy E and Fundenberger J-J 2017 *Ultramicroscopy* **181** 123-133
[34] Zhang T and Britton T B 2024 *Ultramicroscopy* **257** 113902
[35] Cios G, *et al.* 2024 *Ultramicroscopy* **267** 114055
[36] Liu J, Lozano-Perez S, Wilkinson A J and Grovenor C R M 2019 *Ultramicroscopy* **205** 5-12
[37] Cios G, Winkelmann A, Tokarski T, Bednarczyk W and Bała P 2026 *Mater. Characteriz.* **235** 116299
[38] Drouin D, *et al.* *Scanning* **29** 92-101

[39] Wang Y Z, Kong M G, Liu Z W, Lin C C and Zeng Y 2016 *J. Microscopy* **264** 34-40
[40] Sneddon G C, *et al.* 2024 *Ultramicroscopy* **267** 114062
[41] Zaefferer S 2011 *Cryst. Res. Technol.* **46** 607-628
[42] Steinmetz D R and Zaefferer S 2010 *Mater. Sci. Technol.* **26** 640-645
[43] Shen Y, et al. 2019 *Appl. Sci.* **9** 4478
[44] Xing Q 2016 *Scanning* **38** 864-879
[45] Chou C T, Thomsen K, Goulden J and Jiang H 2021 *Microsc. Microanal.* **19** (Supplm. 2) 730-731
[46] AZtecHKL - Nanoanalysis - Oxford Instruments https://nano.oxinst.com/products/aztec/aztechkl
[47] OIM Analysis | EDAX. https://www.edax.com/products/ebsd/oim-analysis
[48] Nanoscale TKD Mapping in the Immersion/UHR Mode of FE-SEMs | Bruker https://www.bruker.com/en/products-and-solutions/elemental-analyzers/eds-wds-ebsd-SEM-Micro-XRF/quantax-ebsd/enabling-nano-scale-tkd-mapping-in-immersion-uhr-mode-of-certain.html
[49] Tong V S, Knowles A J, Dye D and Britton T 2019 *Mater. Charact.* **147** 271-279
[50] Brodusch N, Demers H and Gauvin R 2015 *Ultramicroscopy* **148** 123-131
[51] Brodu E and Bouzy E 2018 *Microsc. Microanal.* **24** 612-613
[52] Vespucci S, *et al.* 2017 *J. Instrumentation* **12** C02075
[53] Wright S I, Nowell M M, de Kloe R, Camus P and Rampton T 2015 *Ultramicroscopy* **148** 132-145
[54] della Ventura N M, *et al.* 2025 *Ultramicroscopy* **276** 114205
[55] Nilsson S, *et al.* 2022 *Phys. Rev. Mater.* **6** 045201
[56] Heinig M F, *et al.* 2022 *Mater. Charact.* **189** 111931
[57] Zhang Y, Schiøtz J and Bastos da Silva Fanta A *BIO Web of Conferences* **129** 07038
[58] Liu B, *et al.* 2026 *Ultramicroscopy* **283** 114333